communications biology

A Nature Portfolio journal

Article

https://doi.org/10.1038/s42003-026-10083-5

Cytometric proteome profiling of GFP-tagged yeast for characterizing novel antifungals

Eslam Ghazy[1,2,3,9], Victoria A. Bidiuk[2,9], Fedor Ryabov[2,4], Olga V. Mitkevich[2], Olga B. Riabova[2], Yaroslav M. Stanishevskiy[3], Igor B. Levshin[5], Liudmila A. Alexandrova[6], Maxim V. Jasko[6], Dmitriy A. Makarov[6], Alexander A. Zhgun[2], Darya A. Avdanina[2], Anna A. Ermolyuk[2], Vitaly V. Kushnirov[2], Anna P. Egorova[2], Michael O. Agaphonov[2] ✉ & Alexander I. Alexandrov[2,7,8] ✉

Assaying cellular responses to antimicrobial molecules is one way to understand modes of action of potential drugs. This is often achieved via transcriptomics and proteomics, but simple, inexpensive methods for rapid characterization are lacking. To bridge this gap, we assayed changes in the abundance of a panel of 64 "sentinel" proteins fused to GFP in the yeast *Saccharomyces cerevisiae* using flow cytometry. This method produced expected patterns for classical antifungals and allowed inference of common mechanisms between known and novel compounds. Single-cell data also revealed diverging responses in mitochondrial protein abundance in response to thiazolidine antifungals, and perturbations of the cell cycle caused by various compounds. Finally, the method provided insight into the unknown mode of action of alkylated nucleosides, which can be used against fungi residing on works of art. These substances elevate levels of proteins involved in the biosynthesis of aromatic amino acids (AAA), as well as in oxidative stress. Furthermore, deficiencies of Trp and Tyr biosynthesis increased the efficacy of these compounds, while antioxidants reduced it. Most surprisingly, antioxidant effectiveness relied on AAA biosynthesis. Thus, our approach and its possible modifications for other microbes provide an easy and reliable platform for revealing modes of action of novel compounds.

Fungal infections kill in excess of 1.5 million people annually, and the emergence of drug-resistant fungi is a global health risk[1]. This is mainly due to the severely limited number of approved classes of antifungal drugs. The main drugs used against systemic mycoses are azoles, which target the lanosterol demethylase Erg11 and inhibit ergosterol biosynthesis; polyenes, which bind ergosterol directly in the membrane; echinocandins, which inhibit glucan-synthase and thus inhibit cell wall synthesis; and flucytosine, which inhibits both transcription and replication. Additionally, there is a wider number of antifungal compounds which are used topically or in industrial applications. An example of such compounds is the copper ionophore zinc pyrithione, which is used in anti-dandruff treatment and in nonmedical applications. For this compound, the influx of copper (or zinc) seems to damage numerous Fe-S proteins[2,3]. Importantly, resistance to nearly all of the compounds used for treatment of systemic mycoses has been reported in all of the standard fungal pathogens, and emerging pathogens, such as *Candida glabrata* and *C. auris* show inherent resistance to these drugs[1]. There is therefore an urgent need to create novel antifungal compounds and decipher their mechanisms of action.

Novel chemicals that affect living organisms are under constant development, including potential pharmaceuticals and drug-like substances, as well as various inhibitors which can be used for scientific research and other purposes. Whether these chemicals were developed rationally or found during non-targeted screens, their effective use and further development requires detailed understanding of the effects on living organisms

[1]Department of Microbiology and Immunology, Faculty of Pharmacy, Tanta University, Tanta, Egypt. [2]Federal Research Center of Biotechnology of the RAS, Moscow, Russia. [3]Institute of Biochemical Technology and Nanotechnology, Peoples' Friendship University of Russia (RUDN), Moscow, Russia. [4]Centre for Biomedical Research and Technology, HSE University, Moscow, Russia. [5]Gause Institute of New Antibiotics, Moscow, Russia. [6]Engelhardt Institute of Molecular Biology RAS, Moscow, Russia. [7]Weizmann Institute of Science, Rehovot, Israel. [8]Department of Molecular and Cellular Biology, Section of Biology, Faculty of Science, University of Geneva, Geneva, Switzerland. [9]These authors contributed equally: Eslam Ghazy, Victoria A. Bidiuk. ✉e-mail: agaphonov@inbi.ras.ru; aleksandr.aleksandrov@unige.ch

and the mechanisms of how these effects are realized. Common approaches to obtain these data are the identification of mutants with resistance or sensitivity to a chemical (which is most suitable for toxic substances)[4], or analysis of the cellular response to chemicals, most often using transcriptomic and mass-spectrometry (MS) based proteomic data (which are applicable to both toxic and nontoxic substances).

Notably, transcriptomics and MS-based proteomics provide very rich data on the response of a cell to a chemical or other treatment involving the quantities of thousands of transcripts or proteins, as well as information on splicing or post-translational modifications. However, these data are often expensive to obtain and analyze, and thus, they can be limited in the number of conditions that can be tested. These approaches also do not easily provide single-cell data on the cellular response to various treatments, which limits the sensitivity and also might prevent observation of important phenomena which occur only in a limited subgroup of cells in a sample population. For instance, a small subset of a population can be persisters[5], i.e., cells with increased tolerance to a drug, which might thus exhibit a distinct response. Also, fungi can form biofilms[6], in which cells are often present in different morphologies, which may also influence resistance to antifungal agents[7] and thus, possibly, response profiles as well. Lastly, observation of responses in single-cell mode can be especially important for compounds that can kill the cells being studied, such as antimicrobials. Nonsecretory proteins can leak out of cells or be excreted during necrotic cell death[8], and thus, measuring their intracellular level would not be informative.

Due to the long available and powerful tools of gene engineering, *S. cerevisiae* is the most thoroughly studied fungus and is among the most studied eukaryotic organisms. Thus, inferring putative mechanisms of action of various compounds, including antifungals, from mutant screening as well as transcriptomic and proteomic responses, as well as follow-up hypothesis testing, using available systematic mutant collections[9], is comparatively easy in this organism. Numerous examples of obtaining useful information on the mechanisms of action of various compounds with antifungal activity have been reported[10,11].

Systematic collections of yeast expressing GFP-tagged proteins[12] are highly informative when used for flow cytometry and have been used for high-throughput flow cytometric studies of various phenomena, such as protein level noise[13], replicative aging[14], as well as more focused studies, such as that of the neighboring gene effect[15]. Thus, this tool is ideal for obtaining single-cell proteomic data. Notably, a recent study has reported the utility of using a limited set of "sentinel proteins" to study the cellular response to stress using targeted MS-based proteomics[16].

The approach we offer and test is based on using flow cytometry to assay changes in the level of a limited set of 64 proteins tagged with GFP, with one strain of yeast being used to assay changes in the level of each protein (Fig. 1A). This array was used to assay the response to 12 compounds, including three compounds used in the treatment of systemic mycoses (fluconazole, voriconazole, and 5-fluorocytosine), a copper ionophore related to zinc pyrithione, and tunicamycin, all of which have known mechanisms of action, as well as several compounds for which the modes of action are unknown. Our results show that the method, termed SCRAPPY (single-cell rapid assay of proteome perturbation in yeast), can be used to rapidly and easily obtain a proteomic profile of the cellular response to a wide range of chemicals. The obtained data show both common responses to a wide range of compounds, as well as compound-specific changes in the proteome. Follow-up study of a novel profile for a group of compounds with an unknown mechanism of action, alkylated cytidines, demonstrated the involvement of aromatic amino acid biosynthesis and oxidative stress, which proved to be interconnected.

Results

Selection of proteins for the test array

Our main goal was to check whether a limited array of *S. cerevisiae* strains producing GFP-tagged proteins would allow observation of clear proteomic signatures for different drugs, as well as to compare them with each other, by monitoring fluorescence of GFP fused to selected sentinel proteins (Fig. 1A). This selection was primarily based on the paper published by the Picotti group[17], in which proteins were selected for MS-based identification based on whether a protein was previously observed in MS data, as well as on the literature suggesting whether or not a protein's abundance characterized a specific cellular process (see Supplementary Data 1). Our selected panel was smaller than that of the Picotti group, since MS can probe changes in abundance as well as post-translational modifications, and we also had a limitation in method sensitivity due to the inability of the flow cytometer to reliably differentiate low GFP levels from cellular autofluorescence[18]. In short, our panel (Supplementary Data 1 and Fig. 1B) included proteins characterizing amino acid biosynthesis and catabolism, DNA repair, carbohydrate metabolism, lipid biosynthesis, oxidative stress, activation of thermotolerance and quiescence pathways. Several proteins not present in the Picotti group's final assay were included, due to their high relevance to antifungal drug responses, such as Pdr5-GFP (a drug efflux pump), Bmh1-GFP, a 14-3-3 protein involved in regulating phosphorylated protein activity, as well as Htb2-GFP, a histone which was recently shown by us to allow monitoring of cell cycle perturbations[19]. Using available data on the GFP-fusion collection[13], we only included proteins that were likely to be observable by flow-cytometry.

Drug selection and treatment optimization

The drugs we selected for testing with the array of strains are listed in Supplementary Data 2, and included two compounds from the azole class, since these are the antifungals of choice in the clinic, and we wanted to compare two compounds with differing structure but with the same target. We also included 5-fluorocytosine, another clinical antifungal, which is a modified nucleotide, and thus could possibly be similar in mechanism with the previously uncharacterized nucleoside analogs[20,21], whose mode of action we also wanted to probe. Zinc pyrithione is a commonly used anti-dandruff agent with antifungal activity, which we also expected to be similar in activity to a novel molecule with antifungal activity, 11326083. Tunicamycin, an inhibitor of secreted protein glycosylation, was selected because it has a known target in yeast and thus its profile could be of interest for comparison with unknown profiles. Mycosidine, a novel topical antifungal compound, was included with its benzoyl derivative to observe differences between profiles of molecules with similar structure. Another tested compound was SDS, since it is commonly used as a membrane/cell wall stressor, and our group has also implicated it in cell cycle perturbations[22]. Bearing in mind that compounds are effective at different concentrations, we used amounts that were based on the minimal inhibitory concentration (MIC). The MICs of the compounds tested were determined for the BY4741 strain (Supplementary Data 2), which is the parent of the GFP-tagged strain collection used in this study. We assumed that MIC or half of the MIC (MIC/2), at which cells can still proliferate, would be sufficient to induce cellular responses. Thus, each drug was tested at two concentrations (MIC and MIC/2), and each test was repeated at least three times.

The time of incubation with the tested compounds should allow the cells to realize their response to the applied stimuli, but should not be too long for technical reasons. Tests with two compounds demonstrated that 6 h was an optimal time for the emergence of a clear response (Fig. S1). Interestingly, we observed protein leakage from dead cells (Fig. S2).

Because GFP tagging can interfere with protein function and thus affect the sensitivity of a specific strain to a drug, we tested the MIC of all of the strains in the panel to several compounds (voriconazole, MP, 11326083, and mycosidine) (Supplementary Data 3). For some of these cases, we could suppose that the proteins in our panel might affect sensitivity (such as the cases of Erg proteins and Pdr5 in azole toxicity, for instance). We observed that for the most part, MICs did not change more than 2-fold (only 2 drug-protein pairs showed 4-fold change of MIC, both for 11326083, which were not key to the obtained profiles). Such a change should not have a serious impact on our ability to construct response profiles for different compounds, also bearing in mind that we tested 2 concentrations for each point.

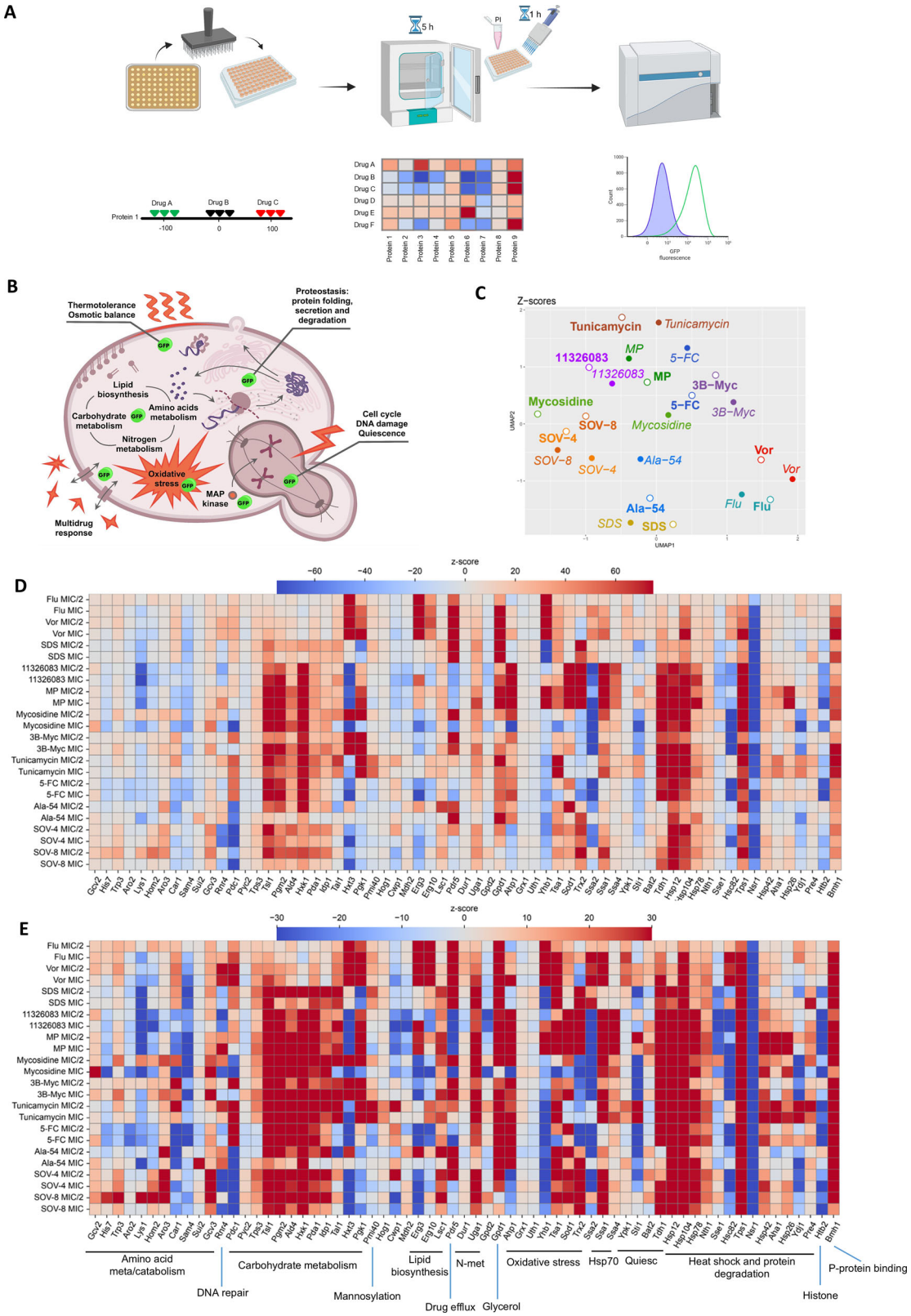

Fig. 1 | SCRAPPY provides clear profiles for various compounds, including classical antifungals, molecules with known targets and novel compounds. **A** Schematic of the SCRAPPY method and data outputs; **B** schematic of the sentinel proteins included into the panel; **C** UMAP representation of distances between averaged Z-score profiles for the tested compounds, empty circles are MIC, filled circles are MIC/2; **D** changes in GFP-fusion protein abundance, using a Z-score metric with a −70/70 scale and **E** a −30/30 scale. Each datapoint was obtained for $n > 3$ independent biological repeats.

However, in the future, this issue might be additionally mitigated by using a modification of a SCRAPPY-panel that consists of diploids that are heterozygous for the GFP-tagged sentinel protein.

General responses to compounds

A bird's-eye view of the obtained data reveals that a considerable number of the selected proteins show upregulation in response to most of the different tested compounds (Fig. 1D, E). For instance, numerous proteins involved in the heat shock response and proteostasis, as well as proteins involved in carbohydrate metabolism, were induced by a number of different substances. Most of the tested stressors elicited this response, which likely relates to the environmental stress response (ESR)[23], indeed, 11 proteins out of the 21 that increase in response to most of our stressors are noted as being involved in the ESR. However, some of our treatments did not induce a classical ESR, as demonstrated by azoles (Flu and Vor) and, to some extent, SDS, both of which show little or only limited induction of chaperones and carbohydrate metabolism genes, respectively.

To determine whether the obtained profiles of protein abundance change allowed clear discrimination between compounds of distinct classes, and similarity between compounds of the same class, we used the Uniform Manifold Approximation and Projection (UMAP)[24] (Fig. 1C) approach to reduce the dimensionality of the data. This approach, somewhat similar to principal component analysis, allows visualization of multidimensional data on a two-dimensional representation. We observed that different concentrations of the same drug are usually close together on the UMAP, as well as drugs from the same class.

Specific proteomic response to the tested drugs

Azoles. An important question was whether the assay revealed specific cellular responses to drugs with known mechanisms of action. Both fluconazole and voriconazole caused robust upregulation of Erg3-GFP and Erg10-GFP, unlike all of the other tested drugs (Figs. 1D and 2A, B). This was consistent with the known mechanism of action of azoles, which involves inhibition of Erg11 and subsequent changes to lipid metabolism. Importantly, deletion of *ERG3* is known to cause resistance to azoles[25], which we confirm independently (Fig. S3A). It is thought that this resistance emerges via preventing the formation of toxic intermediate products of ergosterol biosynthesis, i.e., in this case, increased amounts of Erg3 seem to exemplify a maladaptive cellular response.

As expected, azoles also induced the drug transporter Pdr5 (Fig. 2A, B), which is known to modulate their toxicity by facilitating drug efflux[26] (Fig. S3), although this response is not azole- specific and can be observed for several other compounds in our dataset. We also observed induction of the low-affinity glucose transporter Hxt3 (Fig. 1C), which is induced by both azoles and thiazolidines (see further), however deletion of *HXT3* has no effect on azole toxicity (Fig. S3).

Interestingly, in line with the numerous reports of oxidative stress during azole treatment of fungi[27–32], we observed clear responses for Yhb1 and (to a lesser extent), Tsa1 (Figs. 1C and 2A, B).

Divalent metal ion-transporting molecules—classic and novel

Another substance that we tested was a component of the commonly used anti-dandruff drug zinc pyrithione, 2-mercaptopyridine-*N*-oxide (MP), also known as pyrithione. Zinc pyrithione is known to cause copper and zinc influx into fungal cells[2,33]. This substance, as well as another chemical, synthesized in the course of this project (termed 11326083), is related to a recently tested anti-mycobacterial compound shown to induce copper influx[34]. Both MP and 11326083 demonstrated a very similar response, suggesting that they share a mechanism of action, although several proteins induced by MP were induced less efficiently by 11326083. As expected during copper influx[35], we observed a considerable oxidative stress response (increased levels of Ahp1, Sod1, Trx2) (Fig. 3A, B), as well as the strongest observed induction of the chaperone Ssa4, suggesting proteotoxic stress, likely due to protein oxidation. Notably, both of the compounds seem to cause downregulation of Lys1 (Fig. 1D, E), which is unique among the presented dataset. Notably, this is in line with the known ability of pyrithione to inactivate Fe-S proteins via copper influx[32], including aconitases, which are involved in the early stages of lysine biosynthesis[36].

To confirm that copper influx was the likely mechanism for 11326083, we tested for the induction of Cup1-1-GFP and Cup1-2-GFP, which are metallothioneins involved in copper detoxification. These proteins showed robust induction in the presence of 11326083 and MP (Fig. 3C). Notably, we could observe that protective enzyme induction is much weaker for MIC-equivalent concentrations of 11326083, and the reaction persists to much higher MIC-equivalent concentrations. This suggests that, despite using MIC-equivalent concentrations, the effects of 11326083 are milder than those of MP. These results and the differences between MIC-equivalent profiles of 11326083 and MP suggest the possibility that while the core mode of action of the two compounds likely involves copper ion influx, they probably differ in some more subtle way.

SDS

SDS sensitivity has been extensively used as a stressor, which reveals impairment of the cell wall and/or plasma membrane[37–39], and it has also been implicated in control of the cell cycle[38,40]. In accordance with the previously reported detection of reactive oxygen species using dihydroethidium staining[41], we observed induction of Trx2 (Figs. 1D, E, and 3B). However, despite the fact that SDS-sensitivity is dependent on aromatic amino acid biosynthesis[38,39,41], cells did not upregulate the corresponding proteins, even though alkylated cytidines did so (see further).

Interestingly, SDS was not highly effective in causing upregulation of the chaperones and carbohydrate metabolism proteins, which is observed for most other tested compounds, apart from azoles.

Thiazolidines

For comparison to other drugs, we also performed profiling for two thiazolidine derivatives, which were recently reported in ref. 40. While thiazolidines did not provide as distinct a profile as that of azoles, SDS or copper-influx compounds in terms of uniqueness, mycosidine and 3B-Myc showed induction of the glucose transporter Hxt3 (only at low drug concentration for mycosidine) and drug transporter Pdr5 (Figs. 1D, F, and 4).

Importantly, both Pdr5 and Hxt3 are also induced by azoles (Fig. 1D), with Pdr5 having an important role in azole toxicity (Fig. S3A), which is not the case for mycosidine[40]. As noted above, *HXT3* deletion did not affect the toxicity of Vor (Fig. S3B), but influenced resistance to mycosidine[40], which suggests that for thiazolidines, Hxt3 plays an important role in the mode of action. Interestingly, it has previously been reported that thiazolidine derivatives are efficient blockers of glucose transport[42], though, notably, this paper was later retracted. However, several more reports implicate thiazolidine-based molecules in glucose transport[43,44]. Interestingly, the thiazolidine derivatives used in the clinic are considered to be peroxisome proliferator-activated receptor agonists[45], while these receptors are absent in yeast[46]. This suggests that the effects of thiazolidines may be mediated by other targets in yeast and possibly mammals.

Tunicamycin

Tunicamycin is a known ER-stressor, which inhibits Alg7, a uridine-diphosphate-N-acetyl-glucosamine-1-P transferase catalyzing an essential step of the synthesis of carbohydrate chains, which are attached to asparagine residues of the nascent polypeptide chains translocated into the ER lumen. This is crucial for folding most proteins in this compartment. As could be expected, we observed specific induction of Pmi40 (Fig. 5A, B), which converts fructose-6-phosphate into mannose-6-phosphate required for protein glycosylation in the secretory pathway, and Pre4, which is a subunit of the proteasome, involved in the degradation of damaged ER proteins. Interestingly, tunicamycin also causes strong induction of Tsa1 (Fig. 1), a peroxiredoxin and a partner of Hsp70, which facilitates interaction with oxidatively damaged proteins[47]. Tsa1 was also induced, albeit less dramatically, by the copper-transporting compound MP. We also detected

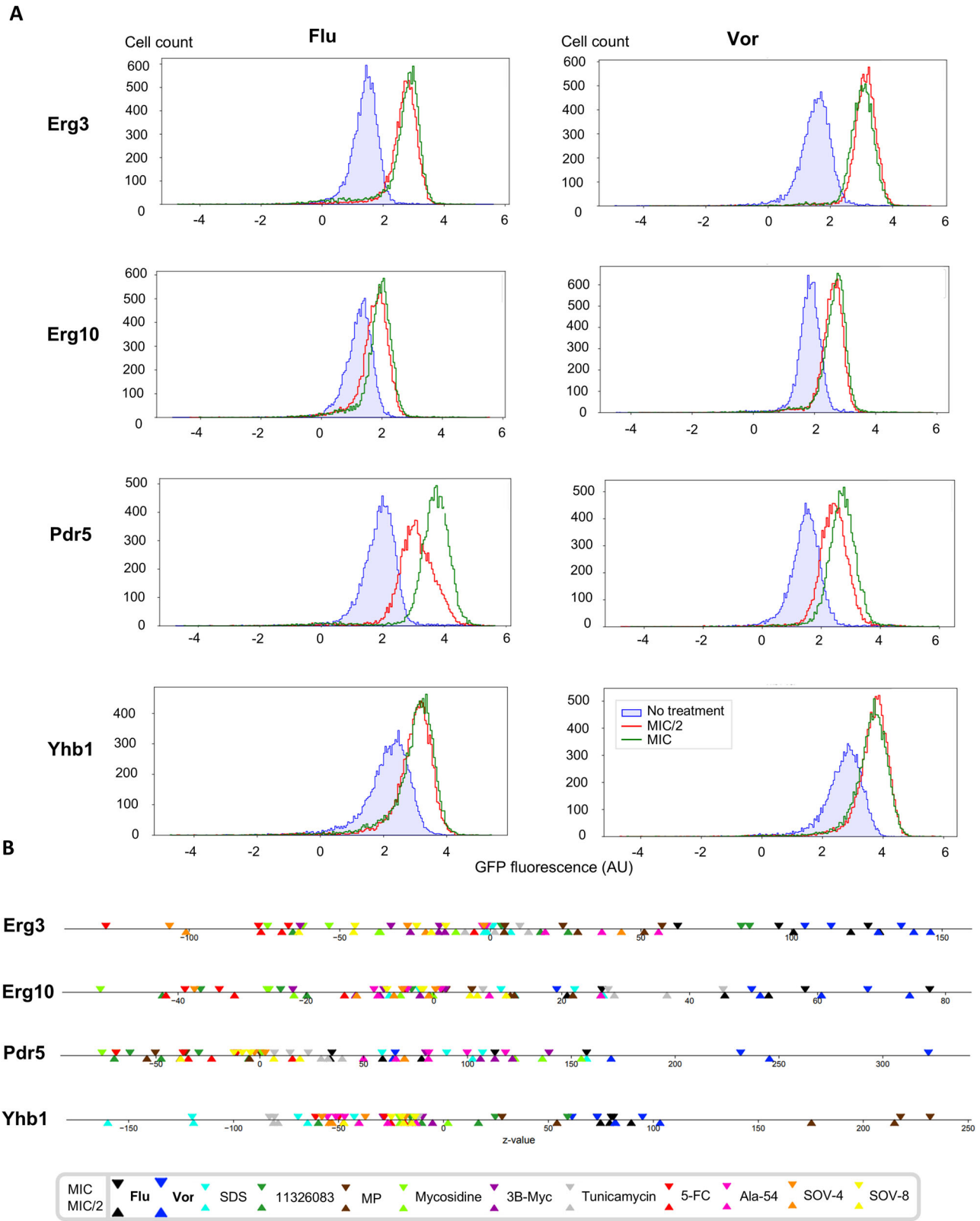

Fig. 2 | SCRAPPY demonstrates the ability of azoles to upregulate lipid biosynthesis enzymes and drug transporters. A Cytometric data on the changes in protein level; **B** comparative unidimensional plot of z-score changes for all tested compounds.

specific induction of Aha1 (Fig. 5) and Ydj1 (Fig. 1D), which are partners of Hsp90s and Hsp70, respectively. These observations highlight the distinct type of proteotoxic oxidative damage triggered by tunicamycin.

Tunicamycin also provides a good test case for determining optimal setups and options for future SCRAPPY modifications. While using the available GFP-fusion collection is highly convenient, some proteins are ill-suited for assay as a C-terminal fusion. For instance, these are proteins possessing C-terminal localization signals, e.g., ER retention signals HDEL or KDEL. One such protein of interest, which might be used as a "sentinel" of the unfolded protein response[48] is Kar2, which is an ER chaperone.

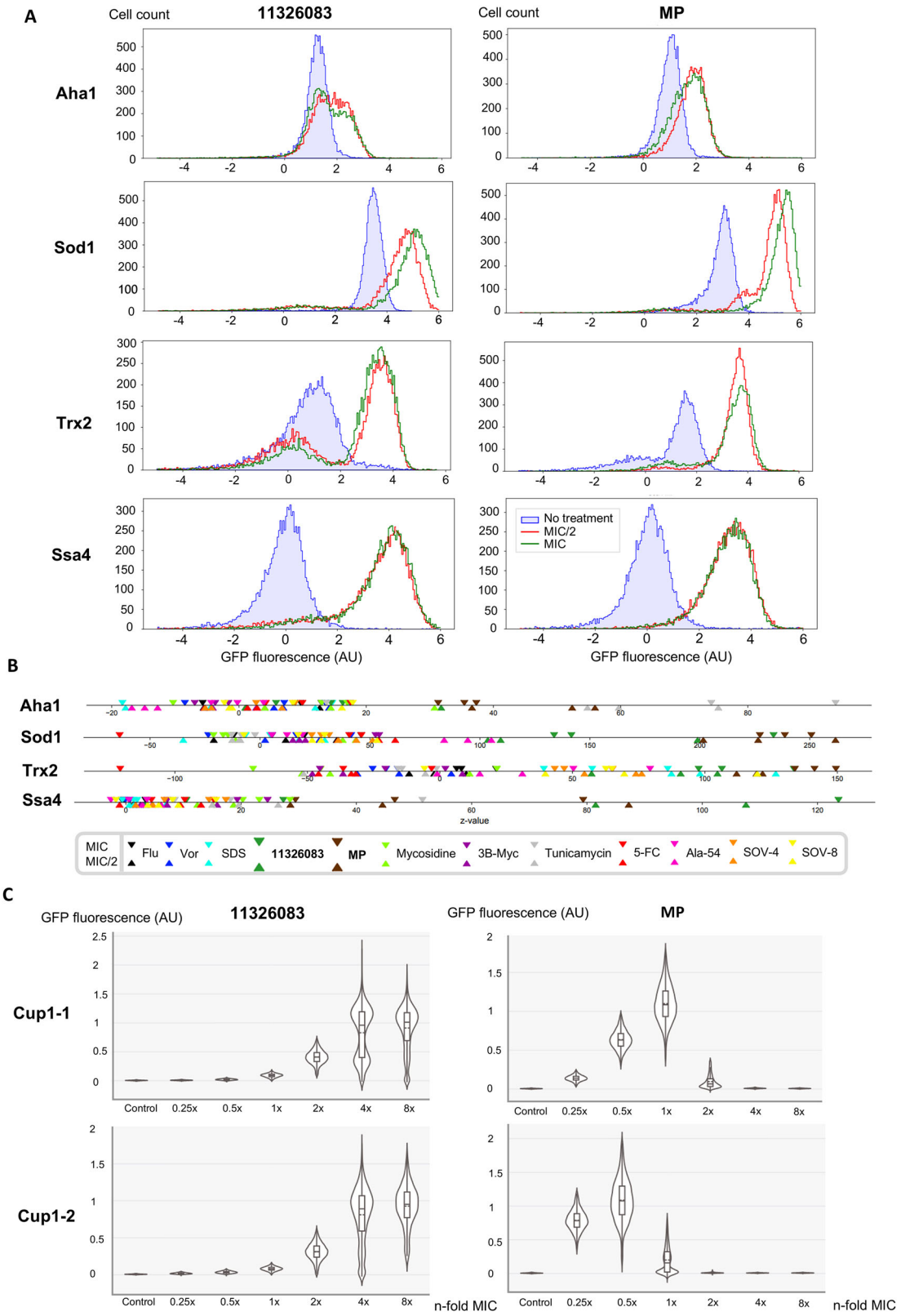

Fig. 3 | MP and 11326083 demonstrate strong induction of the oxidative stress and proteotoxic response, as well as specific induction of copper detoxifying enzymes. A Cytometric data on the changes in protein level; **B** comparative unidimensional plot of z-score changes for all tested compounds; **C** change in the level of Cup1-GFP proteins in response to compound treatment (MICs for 11326083 and MP are noted in Table 1) ($n = 3$ for all experiments in figure, representative distribution shown).

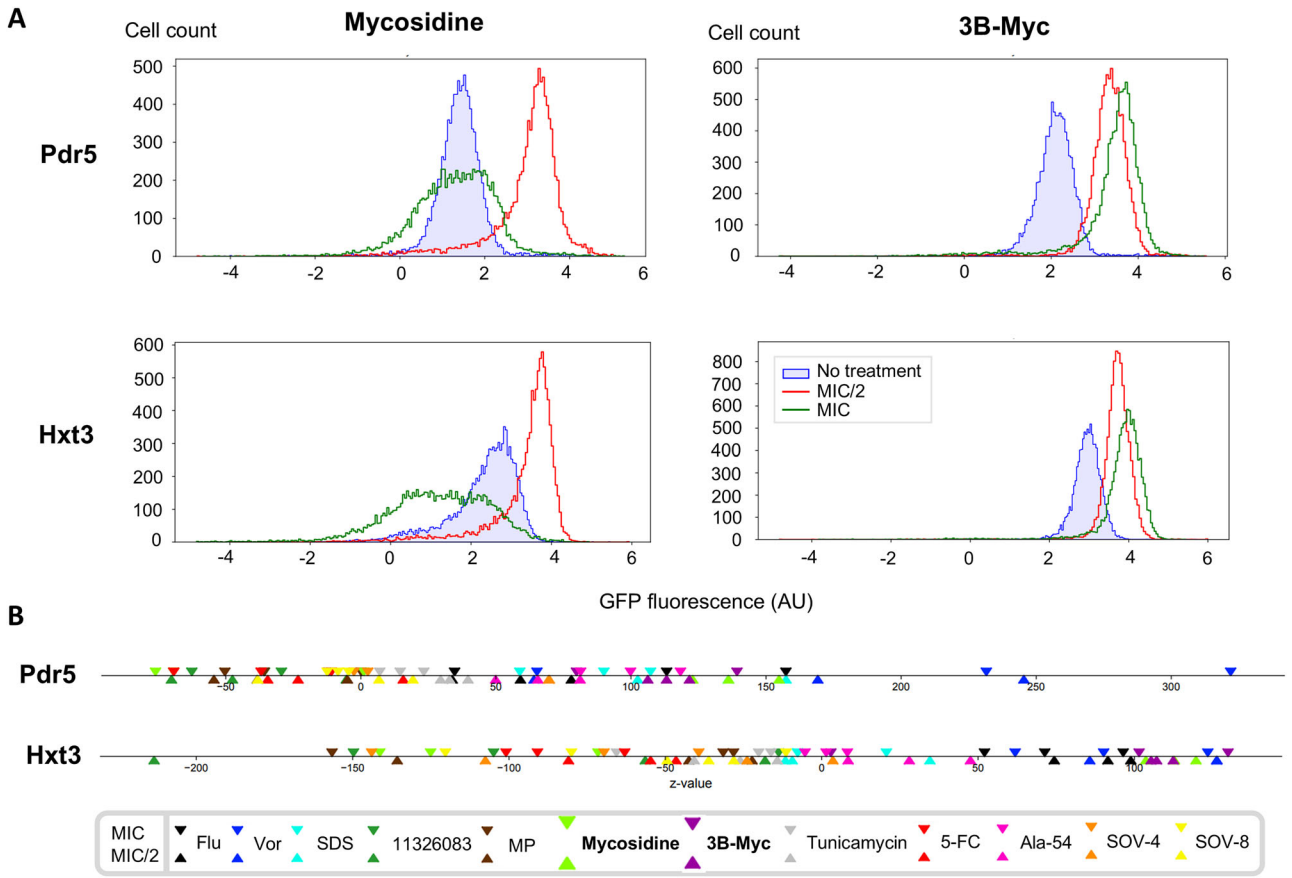

Fig. 4 | Mycosidine and its related compound 3B-Myc specifically induce Hxt3 and Pdr5 levels, showing similarity to azoles. A Cytometric data on the changes in protein level; **B** comparative unidimensional plot of z-score changes for all tested compounds ($n = 3$ for all experiments, representative distributions shown).

Notably, its GFP-fusion (or at least the one present in the GFP-fusion collection available to us) is not localized to the ER, as should be the case for a fully functional protein. This, however, does not, at least in theory, prevent its use as a promoter activity readout.

So, we decided to compare the behavior of this protein with an alternative sentinel setup, where a fluorescent protein (mCherry) was placed under the control of the *KAR2* promoter (P_{KAR2}). Of course, this changes the sentinel readout to be one of transcriptional activation, rather than of increased protein abundance. After treatment with tunicamycin, we observed that while Kar2-GFP did show a weak increase, the response of P_{KAR2}-*mCherry* was far stronger (Fig. 5C).

This demonstrates the potential utility of promoter-based sentinels in the SCRAPPY-like approach, and also that some sentinels can benefit from using promoter-based reporter constructs as opposed to fusion proteins.

Nonhomogeneous change in mitochondrial protein levels

Up to now, we did not utilize the ability of flow cytometry to provide single-cell level data, aside filtering out dead cell data. However, our data can show whether cells in a suspension can respond differently to a treatment. To assess whether this was common, we analyzed fluorescence distributions for each protein and screened the data using polymodality tests in order to detect cases where the distribution of cells was unimodal in the control and multimodal after treatment. While most proteins responded in a homogeneous manner to drug treatment, we observed a bimodal response for the mitochondrial proteins Ald4, Idp1, and Gcv3, as well as the cytosolic hexokinase Hxk1 with high reliability (Figs. 6A and S4). The most robust results were obtained for Ald4 in response to mycosidine (Fig. 6A), but less reliably, also to a range of treatments (5-FC and copper-transporting drugs) (Fig. S4). The response involved some of the cells retaining their baseline level fluorescence, while a considerable portion of cells exhibited increased levels of the protein. Interestingly, other mitochondrial proteins from our panel (Hsp78, Pda1), which did not pass the objective criteria, did show signs of somewhat multimodal distribution in response to mycosidine as well, so this is likely to be a general effect of thiazolidine antifungals on mitochondria (Fig. S4). In order to elaborate on this phenomenon, we used fluorescent microscopy to observe the localization of Ald4 and Idp1 upon treatment with mycosidine. Under control conditions, the proteins had mitochondrial localization (Fig. 6B), which was confirmed by staining with mitochondria-specific dye, LumiTracker Mito Red CMXRos (Fig. S5A). Before treatment, the proteins formed long single string-like structures, while after treatment, for both proteins, we observed obvious changes of mitochondrial morphology, suggesting fission. However, the heterogeneous changes of protein level were only confirmed microscopically for Ald4 (Figs. 6 and S5B). Because glucose transport (Hxt3) is required for adaptation to mycosidine[40], and glucose depletion is known to cause mitochondrial fragmentation at least in fission yeast[49], it is likely that the mechanism of action of mycosidine might involve glucose depletion.

To understand whether these different populations of cells could differ in mycosidine resistance, we conducted sorting of these populations after 6 h of mycosidine treatment at the MIC. Importantly, while preparing the experiments, we realized that heterogeneity was present in the material used for seeding the experiment, i.e., the small colonies used for inoculating medium with and without drug had several distinct populations in terms of Ald4 abundance Fig. 6C, left). Various types of differentiation in yeast colonies have been reported previously, thus such differentiation is not surprising[50–52]. Ald4 population heterogeneity disappeared after cultivation in YPD for 6 h. However, the cell population remained bimodal after mycosidine treatment, with the Top population (higher Ald4 abundance) not changing, and the Bottom population (lower Ald4 abundance) showing induction of Ald4 levels in response to the treatment. Importantly, these two

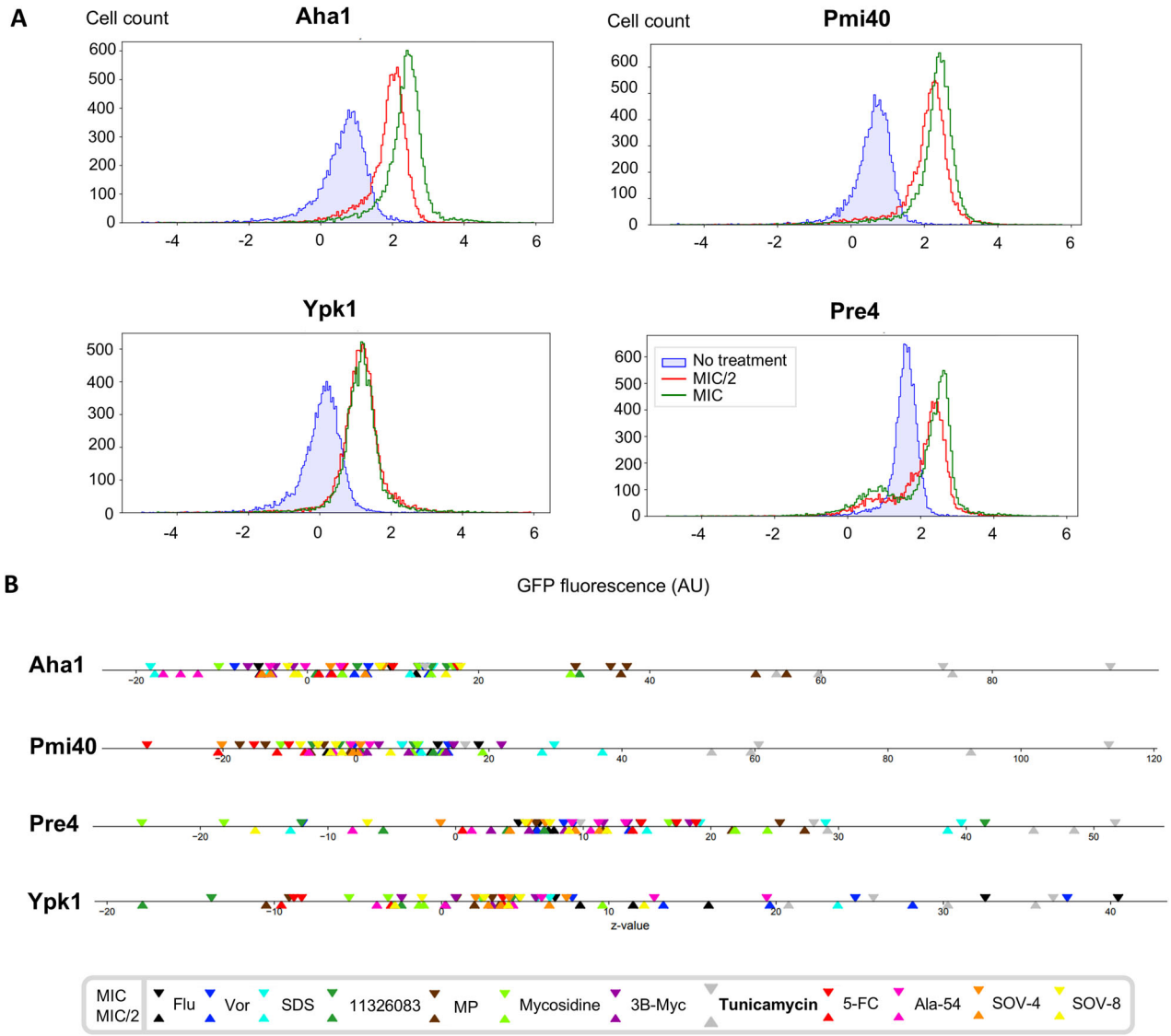

Fig. 5 | Tunicamycin induces specific increases of Pmi40 and Pre4 and induces KAR2 expression, which is detected more reliably using a promoter-activity-based sentinel, rather than a mislocalized GFP-fusion protein. A Cytometric data on the changes in protein level. **B** Comparative unidimensional plot of z-score changes for all tested compounds; **C** responses of KAR2-promoter reporter and Kar2-GFP fusion protein to tunicamycin treatment. Cells harboring RFP under control of the KAR2 promoter (right) or containing the Kar2-GFP fusion protein were grown in medium containing tunicamycin at MIC concentration (2 μg/ml). While the MIC of the Kar2-GFP strain was 2-fold lower than that of the KAR2-promoter strain, the response of Kar2-GFP was strongest at the presented concentration. ($n = 3$ for all experiments, representative distributions shown).

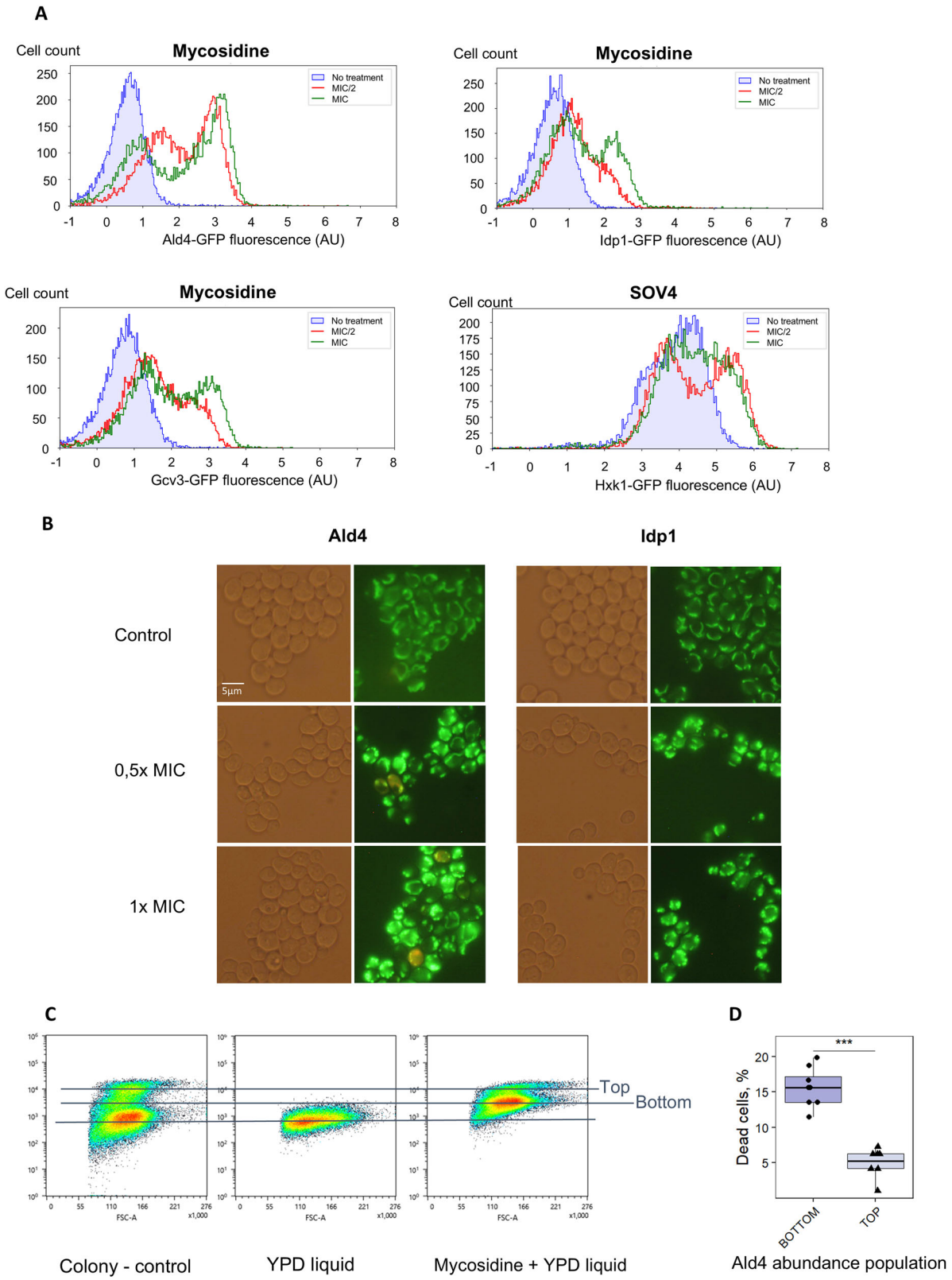

Fig. 6 | Mitochondrial proteins Ald4 and Idp1 display nonhomogeneous changes in response to treatment with mycosidine. A Cytometric data on the changes in protein level; **B** fluorescent microscopy of the same cells used for the cytometric analysis under visible light and GFP fluorescence conditions, treatment with mycosidine ($n = 3$ for experiments in (**A**, **B**), representative distributions and images shown). **C** Flow cytometric data obtained from untreated starting material of the Ald4-mScarlet strain (left), strain incubated for 6 h in YPD (middle) and in YPD with mycosidine (right, MIC concentration). **D** Number of nongrowing cells after sorting of the top and bottom populations, as marked in figure (**C**) Panel **C** shows a representative scatter plot ($n = 3$ biological replicates). For panel **D**: 700 cells per population were sorted (7 sets of 100 cells). The experiment was performed twice with similar results.

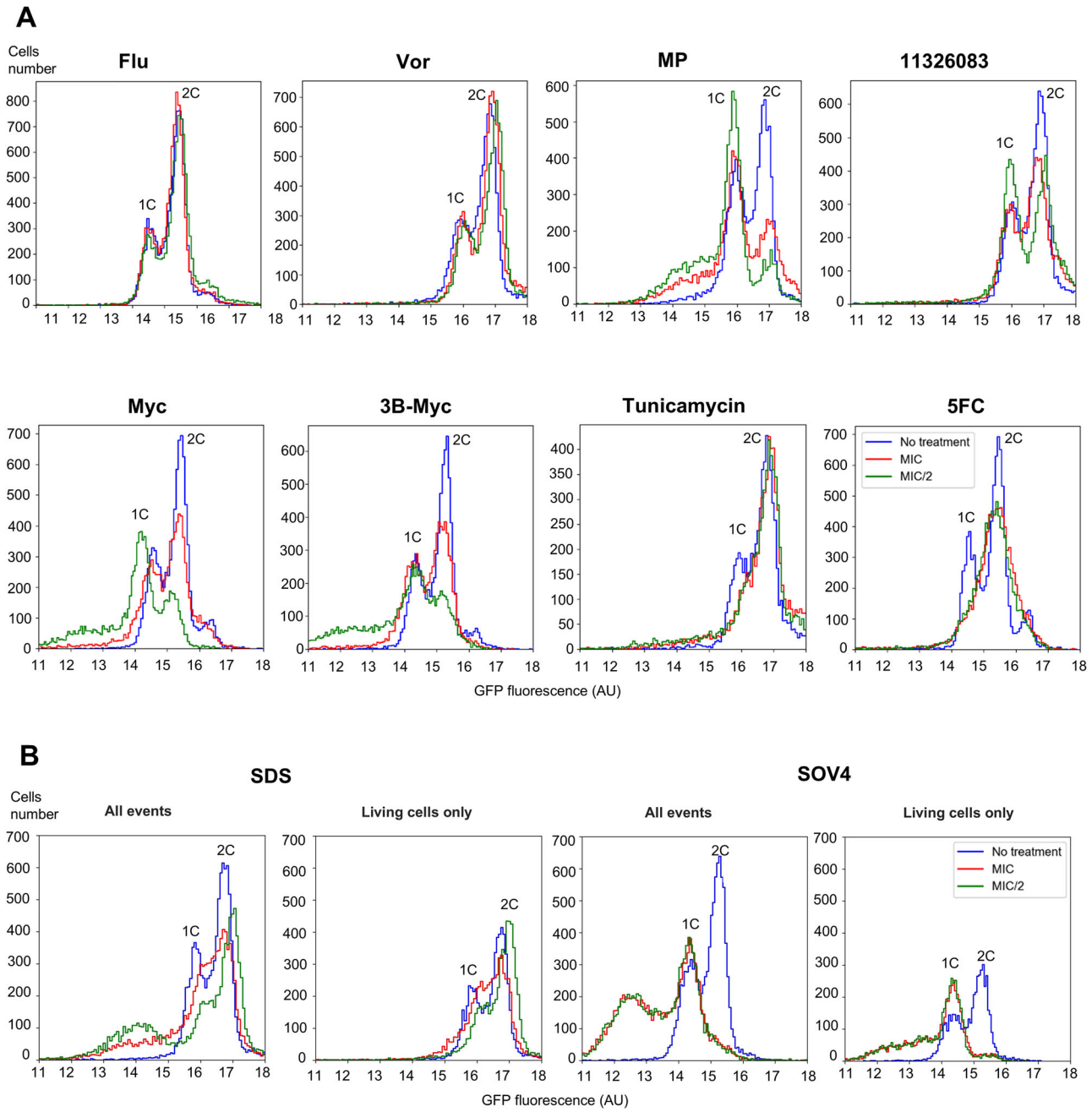

Fig. 7 | Histone abundance quantification using Htb2-GFP reveals effects of antifungal compounds on the cell cycle state of individual yeast cells. **A** Cytometric data on the changes in Htb2-GFP fluorescence in PI-negative cells; **B** cytometric data on the changes in Htb2-GFP fluorescence in PI-negative cells (living cells only panels) and all the cells (all events panels). ($n = 3$, representative distributions presented).

populations differed in their survival to the mycosidine treatment (Fig. 6C). Fluorescent sorting of these two populations showed that the BOTTOM population, despite induction of Ald4, contained approximately 15% nongrowing cells, while the TOP population, which had a high Ald4 level to begin with, had about 5% nongrowing cells (Fig. 6D).

Monitoring effects on the cell cycle

One of the common uses of cytometry is to measure the DNA content of individual cells to characterize the cell cycle. Our recently published method on the use of GFP-tagged histones for cell cycle characterization[19], as well as the inclusion of Htb2-GFP into the SCRAPPY panel, allowed us to easily identify compounds which had an effect on the cell cycle. Because propidium iodide staining was used, we could also analyze only living (PI-negative) cells when needed. As expected, though all of the tested compounds stop cell division, the way in which they do so is not identical. Usually, actively dividing cells exhibit a smaller population of cells with a single complement of DNA (1C) and larger population of cells with replicated DNA (2C), as well as some cells that are replicating their DNA (between these two). We observe that azoles do not change the distribution of histone abundance (Fig. 7A), while thiazolidines and copper ionophore compounds both caused cellular arrest with histone amounts corresponding to 1C. To our knowledge, this is the first report of such an activity for copper ionophores. As expected, and reported previously, 5-FC and tunicamycin caused accumulation of cells in the 2C population[19,53]. SDS seems to cause a delay in the S-phase at lower concentrations and causes cells to pause at 2C if used at MIC. SOV4 resulted in most living cells exhibiting histone abundance corresponding to 1C. Interestingly, since both SDS and SOV4 caused considerable cell death, and we could observe that inclusion of PI-positive

cells revealed a sub-1C peak in the distribution, indicating histone leakage (Fig. 7B). Interestingly, for other compounds where a sub-1C peak was observed, removal of dead cells from the analysis did not remove the peak. Thus, copper ionophores and mycosidine can cause reduction of histone amounts, which might be due to DNA degradation in cells that are impermeable to propidium iodide. This is often interpreted as a sign of apoptosis-like death[27,54].

SCRAPPY provides key information for the characterization of the mode of action of N4-alkyl-cytidines

To demonstrate the usefulness of the SCRAPPY profiles for deeper exploration of a specific class of compounds with an unknown mode of action, we used it to profile the effects of a set of N4-alkyl-cytidines (Ala-54 and SOVs), which can be used to protect works of art from fungal pathogens[20,21]. As a reference, we also obtained SCRAPPY profiles for another nucleic-acid-based antifungal that is used in the clinic, 5-fluorocytosine, 5-FC. We tested 3 SOV compounds, which had differing MICs, including one that had hardly any fungitoxic activity compared to the others, but was used at near the same concentrations for comparison (Supplementary Data 2). The SCRAPPY profiles are presented, and when these are compared with the other compounds, one can observe distinct features: (1) there is notable upregulation of some proteins in the amino acid biosynthesis cluster, namely Hom2, Aro3, and to a lesser extent, Trp3, as well as of the oxidative stress response protein Trx2 (Fig. 8C). Importantly, most of these changes also took place in a hybrid with a prototrophic strain, albeit at a higher concentration, suggesting that the auxotrophic nature of the collection strain does not make much difference in this case (Fig. S6).

SOV-4 and Ala-54 both resulted in upregulation of Pdr5. Notably, while Pdr5 has a minor effect on SOV-4 activity, Ala-54 becomes nearly as toxic as the other derivatives only after PDR5 deletion (Fig. S7). The observation that the role of Pdr5 is influenced by quite a small change (exchange of a -NH_2 for an -OH in the sugar moiety) in the chemical structure is interesting and somewhat unusual.

In order to determine which specific impairments of the amino acid biosynthesis machinery could affect SOV activity, we tested a set of strains with deletions in the amino acid biosynthesis pathways (Fig. S8) and observed that defects in aromatic amino acid biosynthesis had the strongest effects, leading to increased sensitivity (Fig. 8A). Importantly, transport of aromatic amino acids also played a role in the toxicity of SOVs, as deletion of the Tat1 or both the Tat1 and Tat2 permeases increased sensitivity (Fig. 8A). Addition of Trp and Tyr alone decreased sensitivity to SOV in the *trp3*Δ strain, restoring it to WT levels (Fig. 8D). Because our observations showed induction of Trx2, a component of the oxidative stress response, we used two additional methods to confirm the presence of oxidative stress, and its causative role in SOV toxicity. Firstly, we demonstrated that short-term treatment with SOV increased staining with the redox-sensitive dye DCFH-DA (Fig. 8B). Secondly, we assayed the role of antioxidants on SOV toxicity. Addition of antioxidants N-acetylcysteine (NAC) (Fig. 8D), as well as ascorbic acid and glutathione (Fig. S9), reduced the efficacy of SOV on both the wild-type and mutant strains.

Most interestingly, NAC alone was unable to mitigate the effects of SOV in aromatic amino acid biosynthesis mutants, except for *pha2Δ*, which behaves similarly to wild-type in terms of SOV sensitivity. However, NAC was highly effective in reducing SOV activity in the aromatic amino acid transport mutants. This suggests that both transport and synthesis of aromatic amino acids are relevant to maintaining low sensitivity to SOV, but that the effect of an antioxidant cannot help a cell lacking biosynthesis of the aromatic amino acids. This suggests that mitigation of SOV-mediated damage requires both an antioxidant and internal synthesis of Tyr/Trp (Fig. 8D).

Because previous work had shown that various fungi infecting works of art are sensitive to SOV, we decided to examine whether there are indications that in these fungi, the aromatic amino acid pathway (Fig. 8E) was also affected by SOV. For this, we used the filamentous fungus *Penicillium chrysogenum*, strain STG-117, which was isolated from an icon from the Russian State Tretyakov Gallery[55]. The growth of this strain was previously shown to exhibit complete growth inhibition on solid CDA medium containing 0.7 mM SOV4, or SOV8, or Ala-54[20]. In order to observe the effects of growth on subinhibitory concentrations of the compounds, we used a lower concentration (0.2 mM). While this concentration was completely inhibitory for Ala-54, highlighting the differential sensitivity to SOVs between *Penicillium* and *Saccharomyces* (Fig. 8G), slowed growth on the other SOV derivatives (that were also effective in *S. cerevisiae*) was accompanied by accumulation of yellow droplets on the mycelium surface, which are known to contain the pigments chrysogine and others in the same pathway[56] (Fig. 8F). Yellow staining was observed both in the mycelium itself, in the exudate (droplets released on the surface of the mycelium) and also penetrated into the agar medium. Importantly, chrysogine and the other yellow pigments of its biosynthetic pathway are synthesized from anthranilate, a precursor metabolite in the tryptophan biosynthesis pathway, and a derivative of chorismate required for the biosynthesis of tyrosine and phenylalanine. Notably, chrysogine has also been demonstrated to exhibit antioxidant capacity[57]. The obtained data indicate that the effects of SOV on the aromatic amino acid synthesis pathway are conserved across different groups of fungi, and possibly suggests that accumulation of antioxidant metabolites can act as a mechanism of SOV resistance in *Penicillium*.

A possible way in which AAA biosynthesis and resistance to oxidative stress might be connected is via the largely underappreciated cytoprotective antioxidant function of tyrosine and tryptophan residues in transmembrane proteins[58]. Possibly, proteins with such residues might be present in lower amounts in the membrane due to limiting amounts of the AAAs, thereby reducing the capacity of cells to withstand some types of oxidative stress. A wide range of phenotypes has been attributed to deletions in the aromatic amino acid biosynthesis pathway[59], and, possibly, the connection between oxidative stress and this pathway may be the key to understanding this common feature.

Discussion

This study is the first test of a limited chemo-proteomic profiling approach that provides single-cell information. The assay and panel that we have tested show promise as a methodology for rapid testing of various bioactive substances and treatments in terms of understanding their cellular response, and the array of sentinel proteins can be improved and/or tailored to more specific tasks. We show that the profiles obtained by SCRAPPY are reproducible and exhibit high similarity between drugs that have or might have similar mechanisms of action (Fig. 1C), as evidenced by pairs of compounds with known targets (fluconazole and voriconazole) as well as a known drug and a novel molecule (MP and 11326083). We also compared data from SCRAPPY with transcriptomic and proteomic data from treatment with azoles and tunicamycin, respectively[60,61]. This demonstrated that data obtained in similar treatment conditions were quite similar (Spearman's $R = 0.7$ between protein level fold-change after a 6-h tunicamycin treatment). A 15-min treatment with ketoconazole that was analyzed via mRNA-seq, unsurprisingly, did not show overall correlation, however several proteins did show similar increases (Pdr5, Erg3, Erg10, and Yhb1) (Fig. S10).

The usefulness of the SCRAPPY approach in general is highly dependent on the specific sentinels used in the panel, and our results (see Supplementary Data 5) suggests that for the tested substances, more than one-third of the tested sentinels proved useful. However, some of the proteins that either did not respond or showed generalized induction could provide specificity for other compounds. A gap that we feel is worth closing in the future is more sentinels of cell wall stress, as well as the incorporation of some promoter-based sensors, which might mitigate the defective induction of some GFP-tagged proteins (as shown for Kar2).

Overall, we feel that extensive use of SCRAPPY for chemo-proteomic profiling could quite easily provide a database that would allow placing novel substances on a landscape of profiles obtained for previously tested

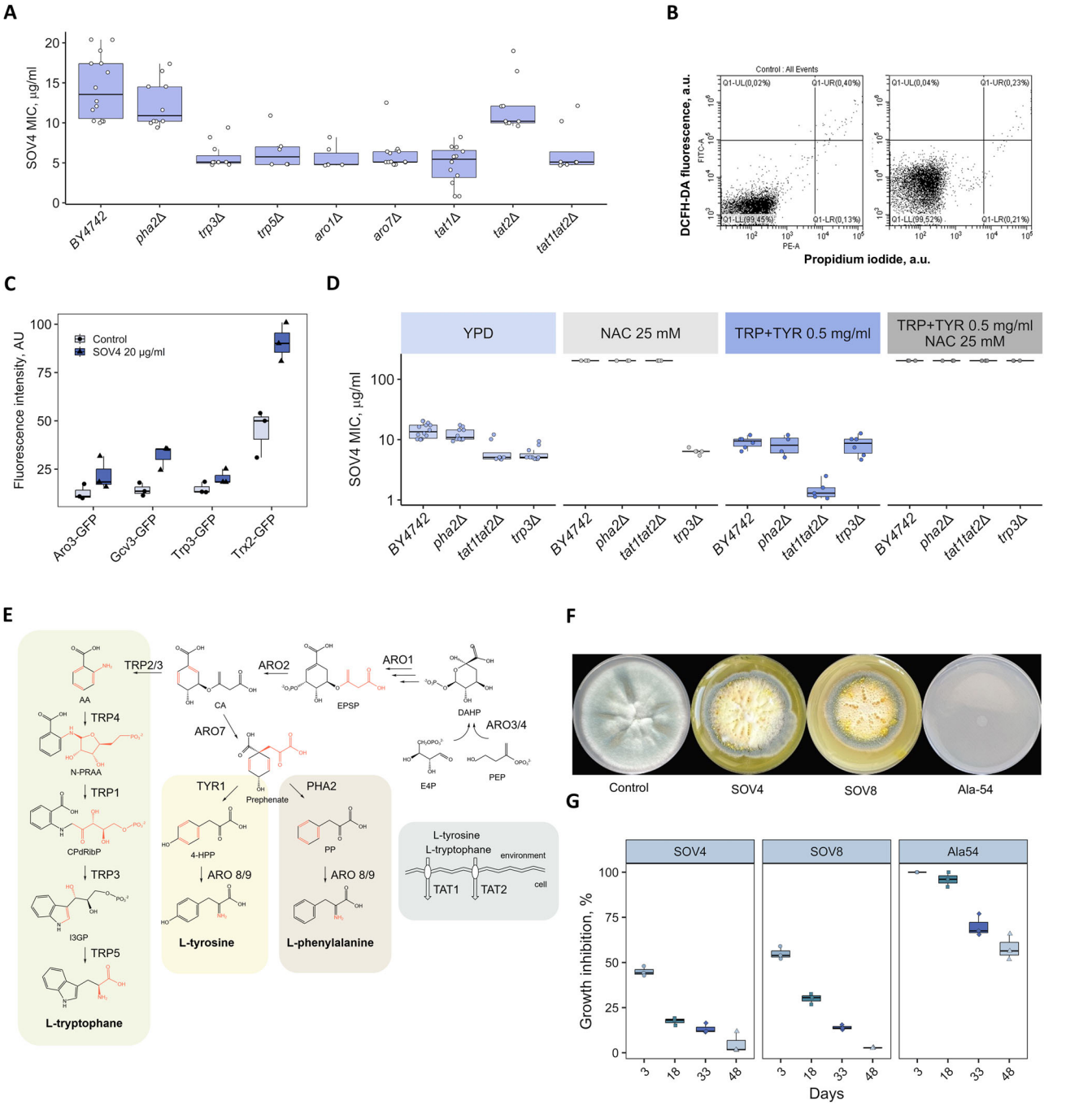

Fig. 8 | N4-alkyl-cytidines induce production of proteins related to aromatic amino acid biosynthesis and oxidative stress, both of which processes are involved in their toxicity. A Yeast strains with deleted genes involved in aromatic amino acid biosynthesis or transport display increased sensitivity to SOV-4 ($n > 5$ for each group); **B** cytometric data for DCFH-DA staining. SOV4 raises ROS level in 15 min after addition to PI-negative cells ($n = 3$, representative scatter plot presented); **C** cytometric data on the changes in protein level for SOV-4 taking into account wild-type cell autofluorescence ($n = 3$); **D** sensitivity to SOV-4 can be effectively mitigated by addition of antioxidants only in the wild-type or aromatic amino acid transport mutant. For strains with disturbed tyr/trp amino acids biosynthesis, this effect can be achieved only with the extra addition of tyr/trp to the incubation medium. NS nonsignificant, i.e., p-value of t-test with WT > 0.05, **-$p < 0.01$. Unnoted are NS for non-marked bars of similar height and <0.01 for bars with dramatic differences. ($n \geq 5$). **E** The aromatic amino acid biosynthetic pathway. Abbreviation of metabolites—E4P erythrose-4-phosphate, PEP phosphoenolpyruvate, DAHP 3-deoxy-D-arabinoheptulosonate7-phosphate, EPSP 5-enolpyruvyl-3-shikimate phosphate, CA chorismic acid, PP phenylpyruvate, 4-HPP p-hydroxyphenylpyruvate, L-PHE L-phenylalanine, L-TYR L-tyrosine, AA anthranilic acid, N-PRAA N-(5-phospho-D-ribosyl)-anthranilate, CPdRibP 1-(2-carboxyphenylamino)-1-deoxy-D-ribulose 5-phosphate, I3GP indole-3-glycerol phosphate, L-TRP L-tryptophan. Red boxes depict genes whose inactivation was shown to increase sensitivity to SOVs, grey—those that were tested and had no effect. **F** The phenotype of *P. chrysogenum* STG-117 colonies after cultivation for 18 days on Czapek-Dox agar (CDA) medium with the addition of 0.2 mM SOV4, or SOV8, or ALA54, or without additives (control). **G** Growth inhibition (%) of STG strains on the CDA medium with the addition of 0.2 mM of SOV4, SOV8, or ALA54. Data acquired at 3, 18, 33 and 48 days after inoculation ($n = 3$).

treatments. It should also be useful for pinpointing a novel substance with a distinct and interesting profile, which would warrant deeper characterization, as exemplified by SOV compounds in our study (Fig. 8).

While the mechanism of action for SOVs is still far from being completely clear, we have conclusively demonstrated that these compounds cause a specific type of oxidative stress (via a currently unknown route), which differs from other oxidative stress-inducing compounds and that aromatic amino acid synthesis is required to survive this stress even in the presence of antioxidants. Further study is required to explore how alkylated cytidines trigger oxidative stress and why it specifically affects aromatic amino acids. A possible scenario, reported in the literature[62] demonstrates that aromatic amino acids in transmembrane domains of proteins can act as antioxidants. If we apply this framework to our situation, mutants in aromatic amino acid biosynthesis and transport can have reduced amounts of transmembrane proteins or reduced rates of their renewal, which could increase sensitivity to SOV. The fact that intracellular aromatic amino acid synthesis was required for antioxidants to mitigate the effects of SOV is intriguing, and one possible explanation for this might be that internal synthesis might more effectively supply aromatic amino acids for incorporation into the membrane (in the form of transmembrane proteins) in a stress situation, rather than external transport, which might be impaired during drug treatment due to damage to transporter proteins or their membrane environment.

One clear challenge for the SCRAPPY method that is currently unsolved is the detection of proteins with low expression levels. This can be approached by testing new, brighter fluorescent proteins, as well as those with spectra in which the background fluorescence is weaker. Another important issue is the time of incubation with the drug, because as of now, we used a 6 h incubation, which can, potentially, miss transient and rapid cellular responses, such as those reported for calcium levels in yeast cells[62]. This could be remedied by fixation of cells with formaldehyde-based reagents, which can retain GFP fluorescence. Importantly, novel fluorescent proteins with higher retention of fluorescence after fixation have also been described in the literature[63,64].

The notable advantages of SCRAPPY are the speed and ease of gathering and analyzing the data, low cost of the assay and moderate consumption of novel bioactive substances, which are often available in limited quantities during the development of lead compounds. These features allow testing multiple treatment conditions for a single substance, which is sometimes prohibitively expensive for omics-based methods. The ability to measure the amount of protein in single cells provides the opportunity of monitoring the effect of compounds on the cell cycle (Fig. 7). It also allows monitoring divergent responses in a cell population, which were demonstrated in this paper for mitochondrial proteins in response to mycosidine treatment. This showcases that SCRAPPY-like methods could be useful for detecting populations of drug-resistant cells, or persisters[5], as well as subtle responses which would otherwise remain unnoticed due to data averaging. Specifically, Ald4 increased in response to many of the tested compounds, and with the averaged data, the response to mycosidine was not unique. However, the multimodal response was characteristic of much fewer drug-protein pairs.

In conclusion, the SCRAPPY method holds significant promise as a rapid and cost-effective tool for chemo-proteomic profiling at the single-cell level, offering the potential to advance our understanding of cellular responses to bioactive substances. Its ability to uncover subtle responses and identify divergent cell populations makes it a valuable and novel asset in the field of drug discovery and cellular biology.

Material and methods

Yeast strains and cell preparation for SCRAPPY

Saccharomyces cerevisiae, strain BY4741 (*MATa his3Δ1 leu2Δ0 met15Δ0 ura3Δ0*) and its derivatives obtained in ref. 16 were used in this work. The array of strains used is available upon request. For MIC determination, the wild-type strain was inoculated into YPD medium (1% yeast extract (w/v), 2% peptone (w/v), 2% glucose (w/v)) supplemented with 2-fold differing concentrations of tested compounds in 96-well plates (200 µL final volume), at an initial OD_{600} of 0.05. Cell growth was judged after 24 h of growth at 30 °C, with the MIC being the lowest concentration of drug where no growth was observed.

Derivatives of the BY4741 strain obtained in ref. 12, harboring C-terminal GFP tags on proteins of interest, were used to detect changes of protein level in response to drug treatment. Genes encoding these proteins were modified in the genome at their 3′-terminus, which corresponds to the C-terminus of the protein, i.e., the regulatory regions of the genes were identical to those of the wild-type proteins. In general, this type of tagging rarely interferes with protein function or regulation[17]. A full table of the strains of *S. cerevisiae* used in this study is presented in Supplementary Data 1. Cells bearing specific GFP fusions were pinned onto solid YPD medium (2% agar) (w/v), grown overnight to form small colonies, and then inoculated into YPD medium containing either no drug with appropriate DMSO concentration, or the tested drug at MIC or MIC/2 concentration, after which the cells were incubated for 6 h prior to flow cytometry. One hour prior to the end of incubation, propidium iodide was added to the incubating cells at a concentration of 1 µg/mL. After this, the control sample and drug-treated sample were analyzed on a Cytoflex S flow cytometer (Beckman Coulter) equipped with a 96-well sampler. GFP fluorescence was assayed using the 488 nm laser and 525/40 FITC filter, whereas propidium iodide staining was assayed with the 532 nm laser and 585/42 PE filter. No less than 10000 cells were acquired for any measurement.

Cultivation of Penicillium chrysogenum

Penicillium chrysogenum STG-117 (MW556011.1) was previously isolated from the surface of the icon "Prophet Solomon" (dated 1731) in the main historical building of the State Tretyakov Gallery (Moscow, Russia). Cultivation of this strain was carried out on Czapek-Dox agar (CDA) medium, formulated with 30 g L^{-1} sucrose, 2 g L^{-1} $NaNO_3$, 1 g L^{-1} K_2HPO_4, 0.5 g L^{-1} $MgSO_4{\cdot}7H_2O$, 0.5 g L^{-1} KCl, 0.01 g L^{-1} $FeSO_4{\cdot}7H_2O$, and 20 g L^{-1} agar, with the final pH adjusted to a range of 7.0–7.4[20,65]. The toxic effect of N4-alkylcytidines (code names-SOVs and Ala-54) on the growth of fungal cells was determined as follows. The cells were collected from agar slants, diluted with 0.9% NaCl to OD_{600} = 0.35 (basic concentration), and sequential ten-fold dilutions in 0.9% NaCl (1.5 µL) were used to inoculate into the center of the petri dishes as previously described with some modifications[66]. The inhibitory effect of the compounds was measured every 3 days for 48 days after inoculation from agar slants onto Petri dishes with CDA, supplemented with 0.2 mM SOV4, or SOV8, or Ala-54 or without additives (control). The percentage of fungal growth inhibition (FGI) was measured according to the formula: FGI% = [(Dc−Dt)/Dc] × 100, where Dc indicates the colony diameter in the control set, and Dt indicates the colony diameter in the treatment set, as described in previous studies. The data recorded were measured in triplicate and repeated at least twice[67].

Cytometry data analysis

Raw data was preliminarily analyzed using CytExpert software (Beckman Coulter). Then it was analyzed using custom Python scripts (https://github.com/fedorrik/scrapper and the https://doi.org/10.6084/m9.figshare.23736219). Comparison of protein levels between treated and control cells was performed using two metrics: fold change of fluorescence and z-score computation. For both options, first, the data obtained by dead cells was filtered (all data with PE-A > 5000 was removed). The protein level was calculated as the level of fluorescence divided by cell size (FITC-A/FSC-A) and the level of autofluorescence (FITC-A/FSC-A of a wild-type strain with no expressed GFP) subtracted. In case of fold change, the median value of protein level of treated cells was divided by the median value of protein level of control cells.

$$\text{Foldchange} = \frac{\text{Med}\left(\frac{\text{FITC}_{\text{GFP}}}{\text{FSC}}\right)_{\text{experiment}} - \text{Med}\left(\frac{\text{FITC}_{\text{Autoflu}}}{\text{FSC}}\right)_{\text{experiment}}}{\text{Med}\left(\frac{\text{FITC}_{\text{GFP}}}{\text{FSC}}\right)_{\text{control}} - \text{Med}\left(\frac{\text{FITC}_{\text{Autoflu}}}{\text{FSC}}\right)_{\text{control}}}$$

Z-scores were calculated as follows:

$$Z = \frac{X_{\text{experiment}} - X_{\text{control}}}{\sqrt{\sigma^2\text{experiment} + \sigma^2\text{control}}}$$

Where

- $X_{\text{experiment}}$ = Med(FITC$_{GFP}$/FSC)$_{experiment}$-Med(FITC $_{Autoflu}$/FSC)$_{experiment}$
- X_{control} = Med(FITC$_{GFP}$/FSC)$_{control}$-Med(FITC$_{Autoflu}$/FSC)$_{control}$
- $\sigma_{\text{experiment}}$ is the standard deviation of experiment sample divided by the square root of the number of data points
- σ_{control} is the standard deviation of the control sample divided by the square root of the number of data points

The cytometry data has been deposited in http://flowrepository.org/,

Analysis of multimodality

To identify heterogeneity of protein level distribution in responses to various treatments, we used two approaches: (1) manual inspection of distributions; (2) computational analysis, which briefly involved searching for cases when there were at least two modes with protein level larger than the control's mode protein level. Modes were detected via Kernel density estimation with Silverman's rule of thumb in Python. Only modes with the maximal cell number or which had cell numbers at least 10% of the maximal one were considered. We also considered reliable only those cases where there were at least two modes equal to or higher than the control's mode in all 3 repeats.

Sorting

Sorting was performed on a SH800S Cell Sorter by Sony Biotechnology (Japan) with a 100-µm microfluidic sorting chip and using the RFP channel to detect protein fluorescence. Cultures of strains with fluorescently tagged Ald4 were grown as described above for the SCRAPPY method and then inoculated into YPD or YPD with a MIC concentration of mycosidine. After incubation for 6 h, the cells were analyzed for fluorescence on the sorter and sorted into 96-well plates with 1 cell per well. Growth of cells in wells was scored after 3 days of growth at 30 °C without shaking.

Microscopy and image analysis

Fluorescence microscopy data was obtained using a Nikon Ti2 inverted microscope and a Nikon DS-Fi3 camera. Cell segmentation was performed using CellPose[68], and mean fluorescence values for each cell were obtained using Fiji[69]. For visualization of mitochondrial morphology by fluorescent dye staining, LumiTracker Mito Red CMXRos, 575/600 nm (Lumiprobe, Russia) was added directly to a 1 ml volume of mycosidine-pretreated cell culture in YEPD to a final concentration of 400 nM. Cells were incubated for 30 min at 30 °C, washed with fresh medium twice and resuspended in YEPD medium. Cells were mounted on a glass slide and imaged immediately.

Synthesis of chemical substances

Supplementary Data 2 presents the data on the compounds characterized in this study.

SOV synthesis

The modified 2′-deoxycytidine derivatives under investigation, N^4-dodecyl-5-methyl-2,-deoxycytidine (Ala-54) and 3′-amino-N^4-dodecyl-5-methyl-2′,3′-dideoxycytidine (SOV4) and 3′-Dimethylamino-N^4-decyl-5methyl-2′,3′-dideoxycytidine (SOV8), were synthesized by methods developed previously[20,21] and described in detail in Supplementary Data 2.

Thiazolidine synthesis

Mycosidine ((Z)-5-(4-chlorobenzylidene)thiazolidine-2,4-dione) and 3B-Myc-(4-chlorobenzylidene)-3-benzoythiazolidine-2,4-dione synthesis was accomplished according to[40] and described in detail in Supplementary Data 2.

Synthesis of ethyl 6-{[[(5-fluoro-2-methylphenyl) amino](imino) methyl]thio-nicotinate 1-oxide hydrochloride (11326083)

(Step a) A solution of ethyl 2-chloronicotinate 1 (1.836 g, 1.0 eqv) and urea hydrogen peroxide adduct (UHP) (1.974 g, 2.1 eqv) in methylene chloride (10 mL) was cooled to 0 °C. Then, TFFA (4.15 g, 2.0 eqv) was slowly added to the solution, and the reaction mixture was stirred at room temperature overnight. The reaction mixture was quenched with water and 0.5 M water hydrochloric acid solution till pH ~ 2, and was then extracted by methylene chloride. The organic phases combined were washed by water, saturated $NaHCO_3$, dried over $MgSO_4$ and evaporated *in vacuo*. The crude ethyl 6-chloronicotinate 1-oxide 2 (1.52 g, 76%) was recrystallized from ethanol. Mass (EI), *m/z* (I_{relat}.(%)): 201.6068 $[M]^+$ (43). $C_8H_8ClNO_3$. ^{1}H NMR (DMSO-d_6; 300 MHz; δ, ppm): 8.94 (s, 1H), 7.81 (dd, 1H, *J* = 8.4), 7.60 (d, 1H, *J* = 8.4), 4.43 (q, 2H, *J* = 7.2), 1.40 (t, 3H, *J* = 7.2).

(Step b) To a solution of 5-fluoro-2-methylaniline 3 (0.650 g, 1.0 eqv) in 1.0 N water hydrochloric acid solution (6.0 mL) was added ammonium thiocyanate (0.435 g, 1.1 eqv) at 100 °C. The resulting mixture was stirred at 100 °C for 16 h and then cooled to room temperature. The solution was then diluted with cold water and neutralized with 28% ammonium hydroxide solution (pH > 7). The precipitate formed was filtered and washed with water and *n*-hexane/diethyl ether to obtain 1-(5-fluoro-2-methylphenyl) thiourea 4 (0.520 g, 46%) as a white solid. Mass (EI), *m/z* (I_{relat}.(%)): 184 $[M]^+$ (65) $C_8H_9FN_2S$. ^{1}H NMR (DMSO-d_6; 300 MHz; δ, ppm): 9.24 (s, 1H), 7.26-7.09 (m, 2H), 7.02-6.94 (m, 1H), 2.14 (s, 3H).

Step c) A solution of ethyl 6-chloronicotinate 1-oxide 2 (0.658 g, 1.00 eqv) and 1-(5-fluoro-2-methylphenyl) thiourea 4 (0.625 g, 1.03 eqv) in acetone was stirred at room temperature for 12 hours. The precipitate formed was filtered and washed with a small volume of acetone. The crude ethyl 6-{[[(5-fluoro-2-methylphenyl) amino](imino)methyl]thio}nicotinate 1-oxide hydrochloride RCB13083 (0.94 g, 83%) was recrystallized from ethanol. Mass (EI), *m/z* (I_{relat}.(%)): 349 $[M]^+$ (56). $C_{16}H_{17}ClFN_3O_3S$. ^{1}H NMR (DMSO-d_6; 300 MHz; δ, ppm): 9.11 (s, 1H), 8.34 (dd, 1H, *J* = 8.4), 8.16 (d, 1H, *J* = 8.4), 7.56–7.46 (m, 2H), 7.18-7.27 (m, 1H), 4.49 (q, 2H, *J* = 7.2), 2.29 (s, 3H), 1.43 (t, 3H, *J* = 7. 2). ^{13}C NMR (DMSO-d_6; δ, ppm): 164.3, 162.4, 156.3, 155.9, 154.5, 140.2, 138.7, 131.8, 131.5, 130.3, 125.6, 125.1, 111.3, 110.6, 109.7, 109.1, 61.1, 17.8, and 14.3.

Creation of the Kar2 promoter-based reporter

The integrative vector pAM978 possessing gene coding for mCherry under control of the *KAR2* promoter was composed of the following DNA fragments: 2237 bp PvuI-EcoRV of pAM784[70], 115 bp PvuII-BamHI of pGAPZalpha (https://www.thermofisher.com/order/catalog/product/V20520), 504 bp BamHI-NcoI (NcoI was filled-in) of PCR product obtained with primers ScPKAR2U and ScPKAR2L and *S. cerevisiae* DNA as a template, 782 bp PCR product obtained with primers ymCherryU and ymCherryL and pAG426-GAL-ccdb-ymCherry (a gift from Susan Lindquist (Addgene plasmid # 14155; http://n2t.net/addgene:14155; RRID: Addgene_14155)), and 1633 bp SmaI-PvuI of pUC18 *E. coli* vector. This plasmid was integrated into the BY4741 genome. To direct the integration into the *KAR2* locus, the plasmid was digested with XhoI, whose site is unique in the plasmid and is located within the *KAR2* promoter. The following primers were used: ScPKAR2L1 ttCCATGGTATGTTTGATACGCTTTTTC; ScPKAR2U1 aaggatccccatgaactcagca; YmCherryU1 gggttaattaacagtaaaggagaagaagacaacatggcaatc; YmCherryL1 GCAGCCCATCACCACTTTG.

Creation of the TAT1/2 deletion strain

A double-deletion mutant, *tat1Δtat2Δ*, was constructed using the tat1Δ strain from Yeast Gene Deletion Collection[9] as a parental strain by disruption of the *TAT2* gene with *HIS3*. The *TAT2* disruption cassette was obtained via PCR using the primers (TAT2:HIS3-D: TTCATATTTGTTTGTATATACATCTGAGCATTGCGGATCTAAATAGTGTGagcgctaggagtcac TAT2::HIS3-R: AATATTCTACAAAAATAAATTGAACTTGTTTCTTCGGTATTAACACCAGAgcgcctcgttcagaatgac) and pRS313 plasmid as a template. Integration of the disruption cassette was assisted by

the CRISPR Cas9 approach. To do this, the plasmid pWS171[11], possessing the guide RNA assembly cassette and *CAS9* encoding gene, was used. The duplex of oligonucleotides Tat2Cr-D (GACTGGCTAGGTGAAAT-CACGGTG) and Tat2Cr-R (AAACCACCGTGATTTCACCTAGCC) were inserted between Esp3I sites of the pWS173 plasmid to direct Cas9 cleavage to the *TAT2* locus. The resulting plasmid was used to co-transform the *tat1*Δ strain with the *TAT2* disruption cassette.

Statistics and reproducibility

All statistical analyses were performed using GraphPad Prism 8 and R version 4.5.0. The data are presented as mean ± standard deviation (SD) or standard error of the mean, unless otherwise stated in the figure legends. For comparisons between two groups, statistical significance was determined using a two-tailed unpaired Student's *t* test or Mann–Whitney test. For comparisons involving more than two groups, a one-way analysis of variance (ANOVA) was performed, followed by Tukey's post hoc test for multiple comparisons. A *p*-value of less than 0.05 was considered statistically significant. Significance levels are denoted in the figures as follows: $^{*}p < 0.05$, $^{**}p < 0.01$, $^{***}p < 0.001$, and $^{****}p < 0.0001$; ns (not significant) indicates $p \geq 0.05$. All experiments were performed at least three times, unless otherwise noted in the figure captions. For microbiological assays, biological replicates were defined as independent yeast colonies obtained from the parental strain after streaking on a solid agar plate. Technical replicates were defined as repeated measurements taken from the same biological sample.

Reporting summary

Further information on research design is available in the Nature Portfolio Reporting Summary linked to this article.

Data availability

All data supporting the findings of this study are available within the paper and its Supplementary Data. List of direct links to deposited cytometry data– http://flowrepository.org/experiments/6888, http://flowrepository.org/experiments/6887, http://flowrepository.org/experiments/6889, http://flowrepository.org/experiments/6890, http://flowrepository.org/experiments/6891, http://flowrepository.org/experiments/6893, http://flowrepository.org/experiments/6892, http://flowrepository.org/experiments/6896, http://flowrepository.org/experiments/6898, http://flowrepository.org/experiments/6897, http://flowrepository.org/experiments/6895, https://doi.org/10.5281/zenodo.18924843. All other materials are available from the corresponding author upon reasonable request.

Code availability

Custom scripts for flow cytometry data analysis and visualization are deposited in https://github.com/fedorrik/scrapper and the https://doi.org/10.6084/m9.figshare.23736219

Received: 17 October 2024; Accepted: 8 April 2026;
Published online: 27 April 2026

References

1. Fisher, M. C. & Denning, D. W. The WHO fungal priority pathogens list as a game-changer. *Nat. Rev. Microbiol.* **21**, 211–212 (2023).
2. Reeder, N. L. et al. Zinc pyrithione inhibits yeast growth through copper influx and inactivation of iron-sulfur proteins. *Antimicrob. Agents Chemother.* **55**, 5753–5760 (2011).
3. Park, M., Cho, Y.-J., Lee, Y. W. & Jung, W. H. Understanding the mechanism of action of the anti-dandruff agent zinc pyrithione against *Malassezia restricta*. *Sci. Rep.* **8**, 12086 (2018).
4. Lee, A. Y. et al. Mapping the cellular response to small molecules using chemogenomic fitness signatures. *Science* **344**, 208–211 (2014).
5. Yaakov, G. Coupling phenotypic persistence to DNA damage increases genetic diversity in severe stress. *Nat. Ecol. Evol.* **1**, 0016 (2017).
6. Ramage, G. et al. Our current clinical understanding of *Candida* biofilms: where are we two decades on? *APMIS* **131**, 636–653 (2023).
7. Harrison, J. J., Ceri, H. & Turner, R. J. Multimetal resistance and tolerance in microbial biofilms. *Nat. Rev. Microbiol.* **5**, 928–938 (2007).
8. Marshall, K. D., Edwards, M. A., Krenz, M., Davis, J. W. & Baines, C. P. Proteomic mapping of proteins released during necrosis and apoptosis from cultured neonatal cardiac myocytes. *Am. J. Physiol. Cell Physiol.* **306**, C639–C647 (2014).
9. Elizabeth, A. & Winzeler, D. Functional characterization of the *S. cerevisiae* genome by gene deletion and parallel analysis. *Science* **285**, 901–906 (1999).
10. Agarwal, A. K. et al. Genome-wide expression profiling of the response to polyene, pyrimidine, azole, and echinocandin antifungal agents in *Saccharomyces cerevisiae*. *J. Biol. Chem.* **278**, 34998–35015 (2003).
11. Anderson, J. B. et al. Mode of selection and experimental evolution of antifungal drug resistance in *Saccharomyces cerevisiae*. *Genetics* **163**, 1287–1298 (2003).
12. Huh, W.-K. et al. Global analysis of protein localization in budding yeast. *Nature* **425**, 686–691 (2003).
13. Newman, J. R. S. et al. Single-cell proteomic analysis of *S. cerevisiae* reveals the architecture of biological noise. *Nature* **441**, 840–846 (2006).
14. Yang, J. et al. Systematic analysis of asymmetric partitioning of yeast proteome between mother and daughter cells reveals 'aging factors' and mechanism of lifespan asymmetry. *Proc. Natl. Acad. Sci. USA*. **112**, 11977–11982 (2015).
15. Egorov, A. A. et al. A standard knockout procedure alters expression of adjacent loci at the translational level. *Nucleic Acids Res.* **49**, 11134–11144 (2021).
16. Soste, M. et al. A sentinel protein assay for simultaneously quantifying cellular processes. *Nat. Methods* **11**, 1045–1048 (2014).
17. Galkina, K. V. et al. Protonophore FCCP provides fitness advantage to PDR-deficient yeast cells. *J. Bioenerg. Biomembr.* **52**, 383–395 (2020).
18. Ho, B., Baryshnikova, A. & Brown, G. W. Unification of protein abundance datasets yields a quantitative saccharomyces cerevisiae proteome. *Cell Syst.* **6**, 192–205.e3 (2018).
19. Kulakova, M. V. et al. Histone abundance quantification via flow cytometry of Htb2-GFP allows easy monitoring of cell cycle perturbations in living yeast cells, comparable to standard DNA staining. *J. Fungi* **9**, 1033 (2023).
20. Alexandrova, L. A. et al. 3′-amino modifications enhance the antifungal properties of N 4-alkyl-5-methylcytidines for potential biocides. *New J. Chem.* **46**, 5614–5626 (2022).
21. Alexandrova, L. A. et al. Discovery of novel N4-alkylcytidines as promising antimicrobial agents. *Eur. J. Med. Chem.* **215**, 113212 (2021).
22. Fokina, A. Inactivation of Pmc1 vacuolar Ca^{2+} ATPase causes G2 cell cycle delay in Hansenula polymorpha. *Cell Cycle* **11**, 778–784 (2012).
23. Causton, H. C. et al. Remodeling of yeast genome expression in response to environmental changes. *Mol. Biol. Cell* **12**, 323–337 (2001).
24. McInnes, L. et al. UMAP: Uniform Manifold Approximation and Projection. *J. open source softw.* **3**, 861 (2018).
25. Watson, P. F., Rose, M. E., Ellis, S. W., England, H. & Kelly, S. L. Defective sterol C5-6 desaturation and azole resistance: a new hypothesis for the mode of action of azole antifungals. *Biochem. Biophys. Res. Commun.* **164**, 1170–1175 (1989).
26. Balzi, E., Wang, M., Leterme, S., Van Dyck, L. & Goffeau, A. PDR5, a novel yeast multidrug resistance conferring transporter controlled by the transcription regulator PDR1. *J. Biol. Chem.* **269**, 2206–2214 (1994).
27. Grosfeld, E. V. et al. A systematic survey of characteristic features of yeast cell death triggered by external factors. *J. Fungi* **7**, 886 (2021).

28. Lee, W. & Lee, D. G. A novel mechanism of fluconazole: fungicidal activity through dose-dependent apoptotic responses in *Candida albicans*. *Microbiology* **164**, 194–204 (2018).
29. Lee, W. & Lee, D. G. Reactive oxygen species modulate itraconazole-induced apoptosis via mitochondrial disruption in *Candida albicans*. *Free Radic. Res.* **52**, 39–50 (2018).
30. Vandenbosch, D., Braeckmans, K., Nelis, H. J. & Coenye, T. Fungicidal activity of miconazole against *Candida* spp. biofilms. *J. Antimicrob. Chemother.* **65**, 694–700 (2010).
31. Belenky, P., Camacho, D. & Collins, J. J. Fungicidal drugs induce a common oxidative-damage cellular death pathway. *Cell Rep*. **3**, 350–358 (2013).
32. Łukowska-Chojnacka, E., Kowalkowska, A., Gizińska, M., Koronkiewicz, M. & Staniszewska, M. Synthesis of tetrazole derivatives bearing pyrrolidine scaffold and evaluation of their antifungal activity against *Candida albicans*. *Eur. J. Med. Chem.* **164**, 106–120 (2019).
33. Leong, C. et al. Effect of zinc pyrithione shampoo treatment on skin commensal *Malassezia*. *Med. Mycol.* **59**, 210–213 (2021).
34. Salina, E. G. et al. Copper-related toxicity in replicating and dormant *Mycobacterium tuberculosis* caused by 1-hydroxy-5-R-pyridine-2 (1 H)-thiones. *Metallomics* **10**, 992–1002 (2018).
35. Shanmuganathan, A., Avery, S. V., Willetts, S. A. & Houghton, J. E. Copper-induced oxidative stress in *Saccharomyces cerevisiae* targets enzymes of the glycolytic pathway. *FEBS Lett.* **556**, 253–259 (2004).
36. Fazius, F., Shelest, E., Gebhardt, P. & Brock, M. The fungal α-aminoadipate pathway for lysine biosynthesis requires two enzymes of the aconitase family for the isomerization of homocitrate to homoisocitrate. *Mol. Microbiol.* **86**, 1508–1530 (2012).
37. Zhao, F. et al. Multiple cellular responses guarantee yeast survival in presence of the cell membrane/wall interfering agent sodium dodecyl sulfate. *Biochem. Biophys. Res. Commun.* **527**, 276–282 (2020).
38. Schroeder, L. & Ikui, A. E. Tryptophan confers resistance to SDS-associated cell membrane stress in *Saccharomyces cerevisiae*. *PLoS ONE* **14**, e0199484 (2019).
39. McClellan, A. J. et al. Yeast require an intact tryptophan biosynthesis pathway and exogenous tryptophan for resistance to sodium dodecyl sulfate. *J Student Res.* **4**, 74–82 (2015).
40. Levshin, I. B. et al. Antifungal thiazolidines: synthesis and biological evaluation of mycosidine congeners. *Pharmaceuticals* **15**, 563 (2022).
41. Cao, C., Cao, Z., Yu, P. & Zhao, Y. Genome-wide identification for genes involved in sodium dodecyl sulfate toxicity in *Saccharomyces cerevisiae*. *BMC Microbiol.* **20**, 1–11 (2020).
42. Wang, D. et al. Development of a novel class of glucose transporter inhibitors. *J. Med. Chem.* **55**, 3827–3836 (2012).
43. Russo, C. D. Peroxisome proliferator-activated receptor γ thiazolidinedione agonists increase glucose metabolism in astrocytes. *J. Biol. Chem.* **278**, 5828–5836 (2003).
44. Hauner, H. The mode of action of thiazolidinediones. *Diabetes Metab. Res. Rev.* **18**, S10 (2002).
45. Thangavel, N., Bratty M. A., Javed, S. A., Ahsan, W. & Alhazmi, H. A. Targeting peroxisome proliferator-activated receptors using thiazolidinediones: strategy for design of novel antidiabetic drugs. *Int. J. Med. Chem.* **2017**, 1069718 (2017).
46. Marcus, S. L., Miyata, K. S., Rachubinski, R. A. & Capone, J. P. Transactivation by PPAR/RXR heterodimers in yeast is potentiated by exogenous fatty acid via a pathway requiring intact peroxisomes. *Gene Expr.* **4**, 227-239 (1995).
47. Hanzén, S. et al. Lifespan control by redox-dependent recruitment of chaperones to misfolded proteins. *Cell* **166**, 140–151 (2016).
48. Lajoie, P., Moir, R. D., Willis, I. M. & Snapp, E. L. Kar2p availability defines distinct forms of endoplasmic reticulum stress in living cells. *Mol. Biol. Cell* **23**, 955–964 (2012).
49. Zheng, F. et al. Glucose starvation induces mitochondrial fragmentation depending on the dynamin GTPase Dnm1/Drp1 in fission yeast. *J. Biol. Chem.* **294**, 17725–17734 (2019).
50. Traven, A. et al. Transcriptional profiling of a yeast colony provides new insight into the heterogeneity of multicellular fungal communities. *PLoS ONE* **7**, e46243 (2012).
51. Palková, Z. & Váchová, L. Cell differentiation, aging, and death in spatially organized yeast communities: mechanisms and consequences. *Cell Death Differ* https://doi.org/10.1038/s41418-025-01485-9 (2025).
52. Váchová, L. et al. Differential stability of Gcn4p controls its cell-specific activity in differentiated yeast colonies. *MBio* **15**, e0068924 (2024).
53. Vai, M., Popolo, L. & Alberghina, L. Effect of tunicamycin on cell cycle progression in budding yeast. *Exp. Cell Res.* **171**, 448–459 (1987).
54. Carmona-Gutierrez, D. et al. Guidelines and recommendations on yeast cell death nomenclature. *Microb. Cell* **5**, 4–31 (2018).
55. Zhgun, A. et al. Detection of potential biodeterioration risks for tempera painting in 16th century exhibits from State Tretyakov Gallery. *PLoS ONE* **15**, e0230591 (2020).
56. Viggiano, A. et al. Pathway for the biosynthesis of the pigment chrysogine by *Penicillium chrysogenum*. *Appl. Environ. Microbiol.* **84**, e02246–17 (2018).
57. Lagashetti, A. C., Dufossé, L., Singh, S. K. & Singh, P. N. Fungal pigments and their prospects in different industries. *Microorganisms* **7**, 604 (2019).
58. Moosmann, B. & Behl, C. Cytoprotective antioxidant function of tyrosine and tryptophan residues in transmembrane proteins. *Eur. J. Biochem.* **267**, 5687–5692 (2000).
59. Turco, G. et al. Global analysis of the yeast knockout phenome. *Sci. Adv.* **9**, eadg5702 (2023).
60. Xiao, H., Smeekens, J. M. & Wu, R. Quantification of tunicamycin-induced protein expression and N-glycosylation changes in yeast. *Analyst* **141**, 3737–3745 (2016).
61. Nishikawa, J. L. et al. Inhibiting fungal multidrug resistance by disrupting an activator-mediator interaction. *Nature* **530**, 485–489 (2016).
62. Kulakova, M. V., Karginov, A. V., Alexandrov, A. I. & Agaphonov, M. O. The GEM-GECO calcium indicator is useable in *Ogataea parapolymorpha* yeast, but aggravates effects of increased cytosolic calcium levels. *Int. J. Mol. Sci.* **23**, 10004 (2022).
63. Campbell, B. C., Paez-Segala, M. G., Looger, L. L., Petsko, G. A. & Liu, C. F. Chemically stable fluorescent proteins for advanced microscopy. *Nat. Methods* **19**, 1612–1621 (2022).
64. Osuga, M., Nishimura, T. & Suetsugu, S. Development of a green reversibly photoswitchable variant of Eos fluorescent protein with fixation resistance. *Mol. Biol. Cell* **32**, br7 (2021).
65. Zhgun, A. A. et al. Search for efficient chitosan-based fungicides to protect the 15th–16th centuries tempera painting in exhibits from the State Tretyakov Gallery. *Microbiology* **89**, 750–755 (2020).
66. Hyvönen, M. T. et al. Hydroxylamine analogue of agmatine: magic bullet for arginine decarboxylase. *Biomolecules* **10**, 406 (2020).
67. Zhgun, A. A., Nuraeva, G. K. & Volkov, I. A. High-yielding lovastatin producer *Aspergillus terreus* shows increased resistance to inhibitors of polyamine biosynthesis. *Appl. Sci.* **10**, 8290 (2020).
68. Stringer, C., Wang, T., Michaelos, M. & Pachitariu, M. Cellpose: a generalist algorithm for cellular segmentation. *Nat. Methods* **18**, 100–106 (2021).
69. Schindelin, J. et al. Fiji: an open-source platform for biological-image analysis. *Nat. Methods* **9**, 676–682 (2012).
70. Agaphonov, M. O. Improvement of a yeast self-excising integrative vector by prevention of expression leakage of the intronated Cre recombinase gene during plasmid maintenance in *Escherichia coli*. *FEMS Microbiol. Lett.* **364**, fnx222 (2017).

Acknowledgements

This work was supported by grants from the Russian Science Foundation-#22-24-00756 (work concerning the development of the SCRAPPY method), #21-74-10115 (work concerning in-depth study of alkylated cytidines in *S. cerevisiae*), #23-14-00106 (design and synthesis of synthetic analogs of alkylated nucleosides), #22-23-00160 (work concerning the design and synthesis of thiazolidine antifungals by IBL). E.G. was funded by a joint scholarship (Executive Program) from the Arab Republic of Egypt and the Russian Federation. Editing and revision of the manuscript were performed by A.I.A. with funding from the Center for Integration in Science of the Ministry of Aliyah, Israel. The work of O.V.M., V.V.K., A.A.Z., D.A.A., and A.A.E. was supported by base funding from the Ministry of Science and Higher Education of the Russian Federation. F.R. was supported by the HSE basic research program. Flow cytometry and final editing of the manuscript during revisions by A.I.A. was supported by the University of Geneva. Flow cytometry was performed at the Shared-Access Equipment Centre "Industrial Biotechnology" of FRC "Fundamentals of Biotechnology" (RAS), Fluorescent sorting was conducted at the ACCESS facility of the University of Geneva with assistance from Stefania Vossio.

Author contributions

E.G. performed SCRAPPY experiments with all the listed compounds, created figures and edited the manuscript. V.A.B. performed studies of SOV after initial SCRAPPY data collection. F.R. analyzed the data and created analysis scripts and created figures. O.V.M., E.G. created constructs and obtained the data on the induction of the Kar2 promoter and protein. O.B.R., A.P.E. synthesized the compound 11326083 and performed preliminary testing of its activity. Y.M.S. edited the manuscript and analyzed the data. I.B.L. synthesized the 3B-Myc and mycosidine compounds and analyzed the data. L.A.A., M.V.J., and D.A.M. synthesized SOVs and analyzed the data. A.A.Z., D.A.A., and A.A.E. performed experiments with filamentous fungi and analyzed the results. V.V.K. devised and implemented the successful strategy in the deletion of aromatic amino acid transporter gene, MOA developed the strategy for creating the Kar2 promoter reporter, contributed to the conception of the project and contributed funding. A.I.A. conceived the project, drafted and edited the manuscript, analyzed data, performed sorting experiments and contributed funding.

Competing interests

The authors declare no competing interests.

Additional information

Supplementary information The online version contains Supplementary material available at https://doi.org/10.1038/s42003-026-10083-5.

Correspondence and requests for materials should be addressed to Michael O. Agaphonov or Alexander I. Alexandrov.

Peer review information *Communications Biology* thanks Miguel Teixeira, Nuno P. Mira and the other anonymous reviewer(s) for their contribution to the peer review of this work. Primary handling editors: Koon Ho Wong and Laura Rodríguez Pérez. A peer review file is available.